RSC Advances

ROYAL SOCIETY OF CHEMISTRY

www.rsc.org/advances

Journal Name

RSCPublishing

ARTICLE

Antifolate-modified Iron Oxide Nanoparticles for targeted Cancer Therapy: Inclusion vs Covalent union

Cite this: DOI: 10.1039/x0xx00000x

Received 00th January 2012,
Accepted 00th January 2012

DOI: 10.1039/x0xx00000x

www.rsc.org/

K. A. López,[a] M. N. Piña,[a] R. Alemany,[b] O. Vögler,[b] F. Barceló,[b] and J. Morey*[a]

In this work four different iron oxide nanoparticles for the delivery of antitumoral drugs into cancer cells were synthesized and characterized. The antifolates Raltitrexed, Pemetrexed and Methotrexate were bound to iron oxide nanoparticles by two different methods: covalent bonding or non-covalent interactions, such as electrostatic and H-bonding. For the covalent bonding of antifolates to the surface of nanoparticles an appropriate linker (3-aminopropyltriethoxysilane) was used, while the non-covalent interaction was achieved with nanoparticles functionalized in one step with squaramides and meso 2,3-dimercaptosuccinic acid. To evaluate the efficacy of the antifolate-derivatized nanoparticles, their cytotoxicity was assayed in A549 human lung adenocarcinoma cells. Only administration of the covalent antifolate-functionalized nanoparticles strongly inhibited the viability of these cancer cells, whereas the delivery of antifolates bound to nanoparticles through non-covalent interactions did not exhibit significant cytotoxic effects. The present results suggest that covalent antifolate-functionalized nanoparticles could be a potential delivery system for certain cancer cells.

Introduction

In the last years, iron oxide nanoparticles have been used as a suitable platform for contrast enhancement in magnetic resonance imaging[1] and as a drug carrier in chemotherapy.[2] Most of these nanoparticles are functionalized with tumor-specific targeting ligands to specifically deliver the anticancer drugs to the tumor cells. One of the strategies used to facilitate the delivery of antitumoral drugs is to conjugate folic acid (FA) to the nanoparticles.[3] The rationale of this approach is that folate-receptors are overexpressed on the cell membranes of many cancer cells compared with normal cells.[4]

The nanoparticle conjugates have the ability to bind to these receptors and, thus, enter the cell via folate receptor-mediated endocytosis.[5] The same cellular mechanism is used by a certain class of antitumoral chemotherapeutics, known as antifolates which are structurally similar to FA, e.g., Methotrexate (MTX), Raltitrexed (RTX) and Pemetrexed (PTX). Despite the cytostatic activity of these antifolates and the established capacity of nanoparticles as drug carriers, only combinations of nanoparticles with MTX[6] have been studied yet.

In general, two different approaches have been explored for drug transportation by nanoparticles. The first consists in conjugating the drugs covalently to the nanoparticle surface through appropriate linkers, and the second, in physically adsorbing or establishing ionic and hydrogen bonds.[3c,7] The covalent method is the most used because the bond strength makes nanoparticle-drug conjugates highly stable. The non-covalent interactions require components that are able to offer donor-acceptor H bonding and ionic interactions and, in this context, squaramides are useful compounds to achieve such associations.[8] In particular, the tetraalkylammonium group of the squaramide substituted derivatives, are capable of tightly binding anions due to the cooperative action of electrostatic and hydrogen interactions (Scheme 1). In fact, in one of our previous studies we described an abiotic squaramide folate binding receptor capable of achieving an affinity high enough for sensing folate-like guests, namely, FA, MTX, PTX and RTX in water.[9] In the practice, we have used the conjunction between squaramides and nanoparticles as a selective receptor for certain carboxylates in an efficient way. However the ability of the squaramide-functionalized iron oxide nanoparticles have not been tested as a possible drug carrier yet.

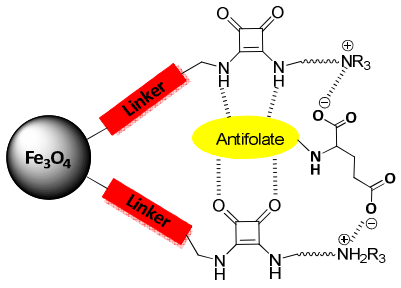

Scheme 1. Possible H bonding and ionic interactions between squaramide derivatives and antifolates.

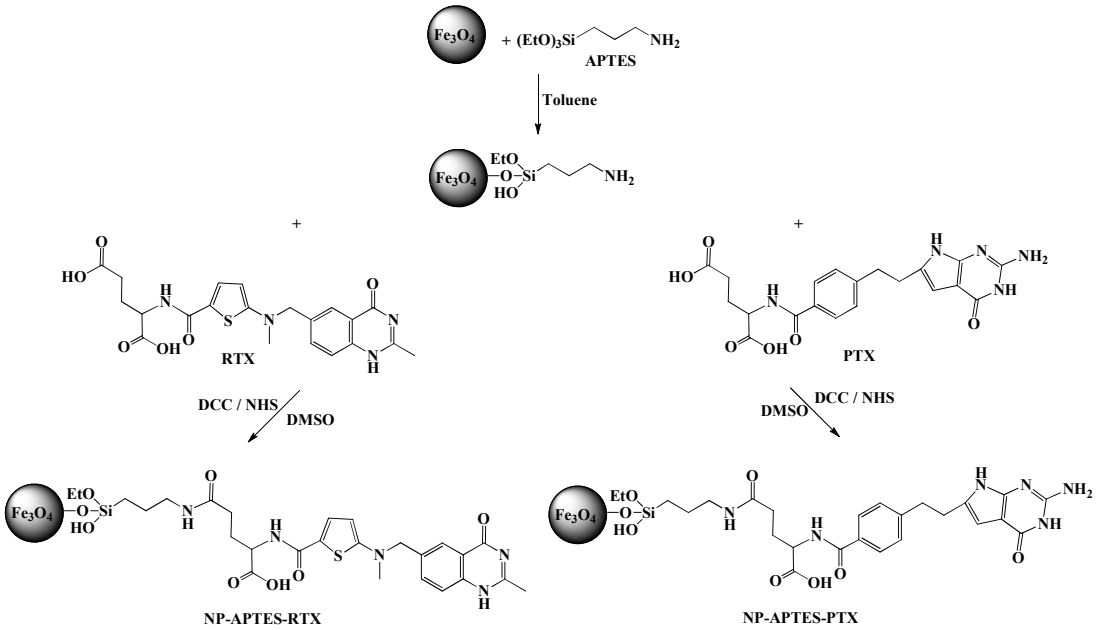

Scheme 2. Synthesis of NP-APTES-RTX and NP-APTES-PTX.

Results and Discussion

The aim of this work was to synthesize and characterize different iron oxide nanoparticles for the transport and delivery of antifolates into cancer cells either through covalent bonding or non-covalent interactions. For the covalent bonding, a common linker 3-aminopropyltriethoxysilane (APTES) was used to react with the antifolates forming an amide bond, whereas for the non-covalent interactions squaramide derivatives were used. Finally, we compared their antitumoral efficacy in A549 human lung adenocarcinoma cells which are known to have folate-receptors overexpressed on their cell membranes.

In order to study the covalent bonding of antifolates, hybrid magnetic nanoparticles NP-APTES-RTX and NP-APTES-PTX were generated. This material was prepared following a previously described method[6a] with some modifications (Scheme 2). Fe_3O_4 nanoparticles were synthesized by thermal decomposition of iron (III) acetylacetonate in the presence of oleylamine, oleic acid and 1,2-hexadecanediol in dibenzyl ether.[10] The surface modification with APTES[11] provided an excellent linker for the subsequent conjugation of RTX or PTX via amidation.

In the context of the non-covalent interactions NP-SQ1 and NP-SQ2 were synthesized (Scheme 3) following a previously described method with minor modifications.[12] Fe_3O_4 nanoparticles, obtained as described above, were surface-modified with meso 2,3-dimercaptosuccinic acid (DMSA) and the corresponding squaramides SQ1 or SQ2[13] in one step. DMSA[14] increases the solubility of nanoparticles making them completely water-soluble. Besides, the terminal amine or ammonium salt in SQ1 and SQ2 respectively, are positively charged at pH 7.4, hence, facilitating the interaction with the carboxylic groups of the antifolates that are deprotonated at this pH.

The correct surface modification of NP-APTES-RTX, NP-APTES-PTX, NP-SQ1 and NP-SQ2 was confirmed by FTIR spectroscopy (Fig. 1). The presence of C=O stretching bands at 1625-1630 cm^{-1} and the amide N-H bands at 1555-1560 cm^{-1} as well as the Si-O bonding peaks at 1000 cm^{-1} in the spectrum, confirm the presence of the antifolates bound to the surface. On the other hand, the squaramide coating of NP-SQ1 and NP-SQ2 was confirmed with typical C=O stretching bands at 1800 cm^{-1}. The amide N-H bend peak at 1590 cm^{-1} was also attributed to coated squaramide. The peak at 1370 cm^{-1} attributed to the symmetric stretch band of the carboxylate (COO^-) confirmed the presence of DMSA. An Energy-dispersive X-ray (EDX) performed to NP-APTES-RTX and NP-SQ1 showed the presence of Si and S (Fig. 1A and 1C insert).

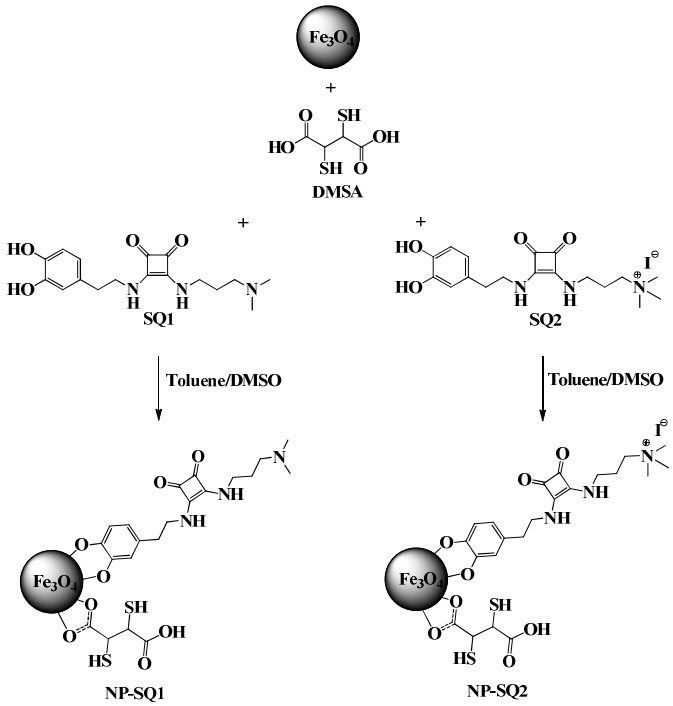

Scheme 3. Synthesis of NP-SQ1 and NP-SQ2.

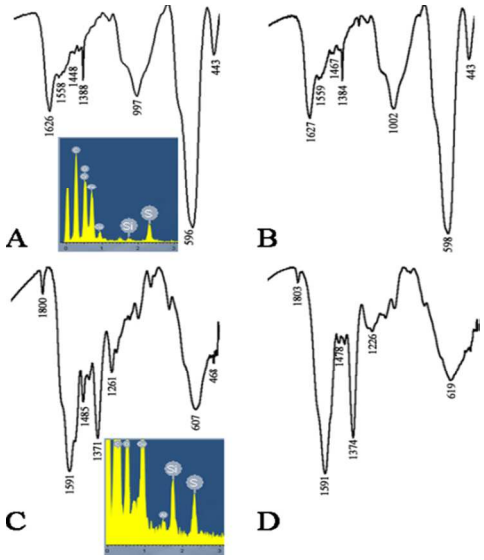

Fig. 1. FTIR and EDX characterization of A) NP-APTES-RTX, B) NP-APTES-PTX, C) NP-SQ1 and D) NP-SQ2.

The uniform shape and size distribution of the different particles (Fig. 2) was analyzed by transmission electron microscopy (TEM) and showed an iron oxide core of about 8 nm. Dynamic light scattering (DLS) studies (Fig. 2 insert) indicated the presence of stable nanoparticles with a hydrodynamic diameter of 70 and 80 nm for NP-APTES-RTX and NP-APTES-PTX. The polydispersity index (PDI) obtained for these nanoparticles was 0.43 and 0.41 respectively. These values showed a mid-range polydispersity. A hydrodynamic diameter of 90 and 120 nm was obtained for NP-SQ1 and NP-SQ2. In this case PDI values were 0.21 and 0.26 respectively, which placed these nanoparticles in an intermediate range of polydispersity.

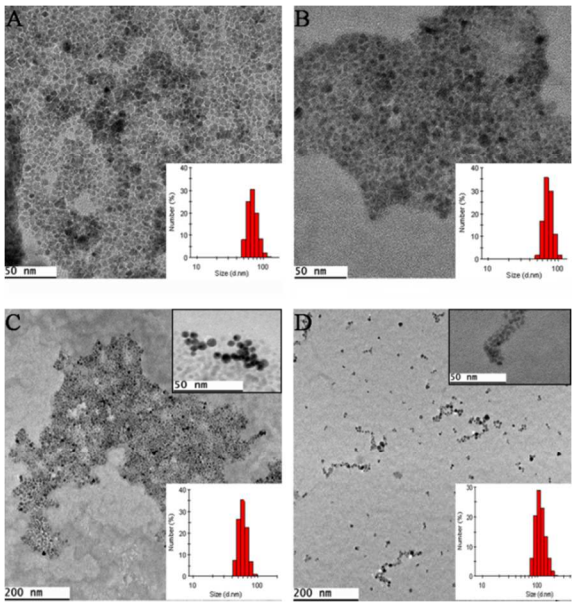

Fig. 2 TEM and DLS characterization of A) NP-APTES-RTX, B) NP-APTES-PTX, C) NP-SQ1 and D) NP-SQ2.

The different nanoparticles were also characterized by Zeta potential. For NP-APTES-RTX and NP-APTES-PTX an average of -8.3 and -7.9 mV was obtained at pH=7.4. For NP-SQ1 and NP-SQ2 Zeta potential values were measured as a function of pH (Fig. 3). The results showed that these nanoparticles had a significant negative charge at pH=4 due to the presence of the carboxylic groups of DMSA. For NP-SQ1 a gradual decrease of Zeta potential between pH 4 and 8.4 was observed as a result of the complete deprotonation of carboxylic groups of DMSA and the partial deprotonation of thiol and amine groups from DMSA and squaramide respectively. Instead, for NP-SQ2 a decrease of Zeta potential value was observed only between pH 4 and 7.4 due to the deprotonation of carboxylic and thiol groups from DMSA. At higher pH, Zeta potential value remains constant because of the tetraalkylammonium salt of squaramide SQ2.

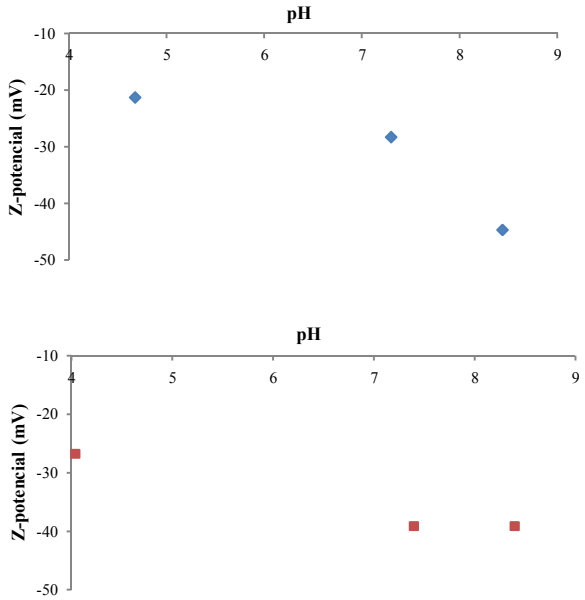

Fig. 3. Zeta potential values of NP-SQ1 (above) and NP-SQ2 (below) as a function of pH. Values obtained from a solution of 0.028 mg Fe/mL of each nanoparticle in a 0.01 M NaCl solution.

Once NP-APTES-RTX and NP-APTES-PTX are taken up by the cells, the molecular mechanism to release the covalent bound antifolates involves lysosomal proteases. Lysosomal proteases are able to hydrolize peptide-like amide bonds (such as the covalent bond with which the antifolates are conjugated to the nanoparticles), thereby releasing these drugs into the cytoplasm.[15] The intracellular lysosomal conditions were simulated in vitro using a crude protease extract and incubating it at 37 ºC with NP-APTES-RTX and NP-APTES-PTX at different pH (4.0, 5.6 and 7.4) and time periods (24 – 96 h). The maximum release of RTX and PTX was quantified by HPLC analysis.[16] As shown in Fig. 4 a decrease in the pH increased the release of RTX or PTX from the nanoparticles, which is in line with the higher activity of lysosomal proteases at lower pHs. These results also revealed that the maximum possible amount of drug was already released after 24 h with the release of RTX being higher than that of PTX. This fact was related with the initially higher concentration of RTX bound to the nanoparticle´s surface compared to PTX. The release of RTX and PTX observed at higher pHs, specifically 5.6 and 7.4, was due to the residual activity of the mentioned proteases and their large amount compared to the functionalized nanoparticles in this assay. Previous drug release experiments with MTX

covalently bound to iron oxide nanoparticles showed the same tendency.[6a] The maximum quantity of RTX and PTX released was 0.445 ± 0.001 µmol/mg Fe and 0.027 ± 0.001 µmol/mg Fe, respectively, at pH 4.0.

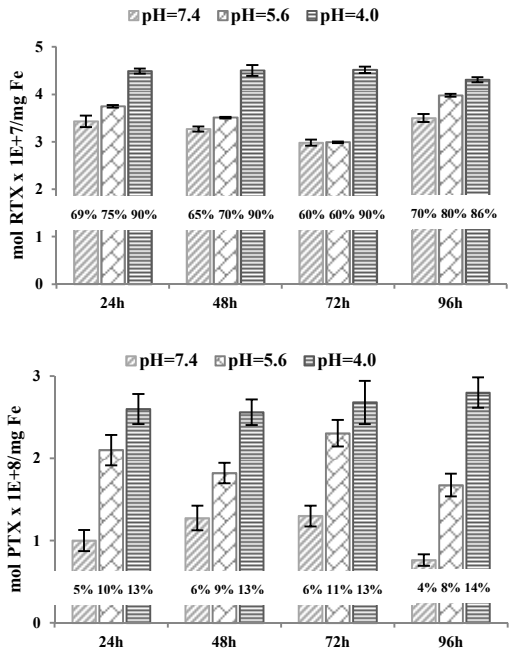

Fig. 4. Covalently bound Raltitrexed (above) and Pemetrexed (below) released from nanoparticles at different pH and time periods at 37 ºC using a crude protease extract. Percentage of drug released at each pH and time is included on each column. Drug release was measured by HPLC.

The concentration of RTX and PTX covalently bound to the iron oxide nanoparticles via amidation was estimated by ^{1}H-RMN through the residues of the reaction. The initial quantity of RTX and PTX present on the nanoparticle´s surface was about 0.5 µmol/mg Fe and 0.2 µmol/mg Fe, respectively. This result suggested that the release of RTX reached 90% while for PTX reached only 14%. This fact demonstrated that the hydrolysis of the peptide-like amide bonds of RTX was more effective in these experimental conditions. The lower release of PTX was not considered negative. Previous drug release assays performed in similar experimental conditions with MTX[6d,17] showed a significantly lower release of this antifolate, without affecting the final cytotoxicity of the functionalized nanoparticles.

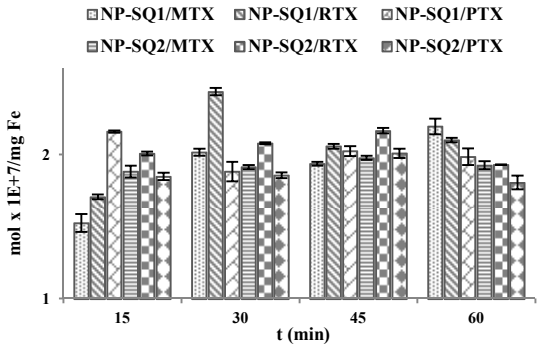

Fig. 5. Antifolate retention by NP-SQ1 and NP-SQ2 measured by HPLC.

The retention and release of RTX, PTX and also MTX from NP-SQ1 and NP-SQ2 was measured by HPLC. The retention process was studied at pH 7.4 in PBS (phosphate buffered saline) buffer at different times (15, 30, 45 and 60 min). The results suggest that RTX, PTX or MTX were retained to a similar extent at the same concentration (about 0.2 µmol/mg Fe) by both types of nanoparticles. In addition, time did not affect antifolate retention as shown in Fig. 5.

The release of antifolates was also analyzed by HPLC at pH 7.4 and 4.0. The results showed that up to 5-15% of the total amount of both drugs was released at pH 7.4, while the release increased up to 90% at pH 4.0 (Fig. 6). At this last pH the carboxylic groups of the different antifolates are protonated. This fact affects the formation of ionic interactions with the ammonium salts of the squaramides SQ1 and SQ2 and causes the release of the antifolates. The released amount was quantified and results are shown in Table 1.

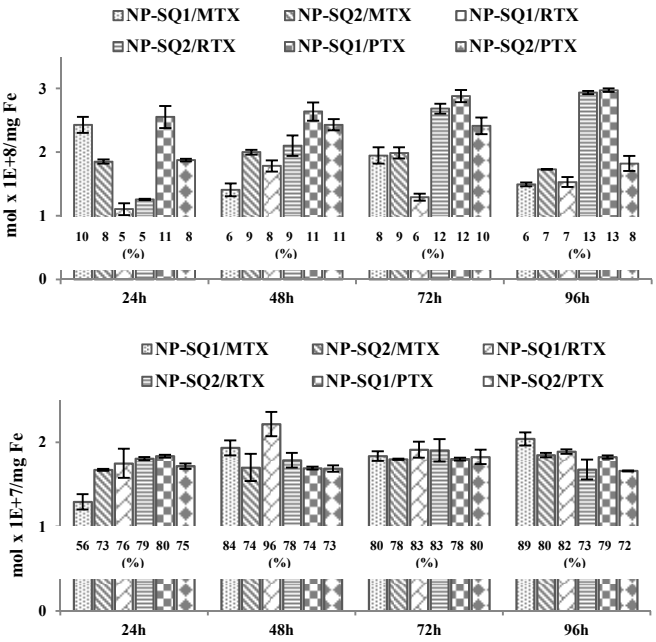

Fig. 6. RTX, PTX and MTX release from squaramide-functionalized nanoparticles NP-SQ1 and NP-SQ2 at pH=7.4 (above) and pH=4.0 (below), measured by HPLC. Percentage of drug released at each time is included on each column.

Table 1 Quantification of the maximum antifolate release by NP-SQ1 and NP-SQ2

	NP-SQ1[a]	NP-SQ2[a]
MTX	0.18 ± 0.03	0.18 ± 0.01
RTX	0.19 ± 0.02	0.18 ± 0.01
PTX	0.18 ± 0.01	0.17 ± 0.01

[a] µmol/mg Fe

Cytotoxicity Studies

The potential cytotoxicity of the nanoparticles conjugates was evaluated in vitro in A549 cells using the MTT[18] assay to compare the efficacy between the different antifolate drugs bound to nanoparticles through covalent binding or through non-covalent interactions, like H-bonding and electrostatic forces. A549 cells are known to have folate receptors overexpressed on their cell membranes.

Fig. 7, 8 and 10 show the time-course of viability of A549 cells as percentage of cell survival after treatment with soluble antifolates or the respective antifolate-functionalized nanoparticles. The cellular viability in the presence of both soluble RTX or PTX and NP-APTES-RTX was found strongly reduced after 96 h as indicative of the cytotoxicity of both antitumoral drug delivery strategies. However, soluble RTX and PTX (Fig. 7) showed a high differential dose-dependent cytotoxicity after 96 h of treatment. While soluble RTX strongly inhibited cell viability up to 58 ± 4% at 25 nM, reaching a maximum inhibition of 84 ± 2% at 0.1 μM, PTX only reduced cell viability by 57 ± 3% at 1 μM, the maximum drug concentration studied.

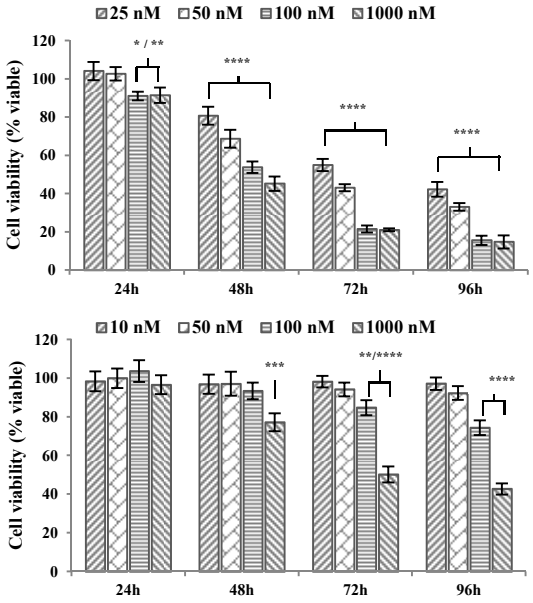

Fig. 7. Cell viability in A549 cells after treatment with soluble RTX (above) and soluble PTX (below) at different time periods and concentrations. Each column represents the mean ± SE of three independent experiments performed in triplicate normalized to non-treated cells (taken as 100%). ***P*< 0.01, ****P*< 0.001 and *****P*< 0.0001 versus non-treated cells.

Similar results were obtained after treatment of tumor cells with RTX or PTX covalently bound to nanoparticles (Fig. 8). NP-APTES-RTX inhibited A549 viability in a dose-dependent manner, reaching a maximum inhibition up to 78 ± 1% at a concentration of 0.005 mg Fe/mL after 96 h of treatment. Higher concentrations of NP-APTES-RTX did not cause a stronger reduction of cell viability. Interestingly, treatment of cells with the same concentration of NP-APTES-PTX did not affect A549 cell viability in the same extent.

The poor anti-tumoral efficacy exhibited by NP-APTES-PTX indicates that the maximum amount of PTX that could be released from these nanoparticles into the cells was not sufficient to affect cell viability. In agreement with this observation, the maximum release of free PTX that could be reached by the highest concentration of NP-APTES-PTX (0.01 mg Fe/mL) studied was only about 0.27 μM, a concentration that provoked only a mild effect on cell viability when administered as soluble drug (Fig. 7 below). This implies that a higher concentration of PTX at the nanoparticle´s surface or a higher release of it would be needed to obtain a notable reduction in cell viability.

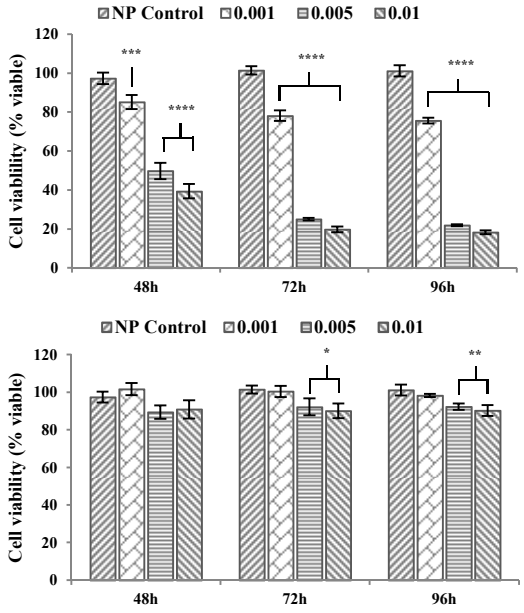

Fig. 8. Cell viability in A549 cells after treatment with NP-APTES-RTX (above) and NP-APTES-PTX (below) at different time periods and concentrations. The NP concentrations are expressed as mg Fe/mL. NP-APTES was used as control (NP Control) at a concentration of 0.01 mg Fe/mL. Each column represents the mean ± SE of three independent experiments performed in triplicate normalized to non-treated cells (taken as 100%). **P*< 0.05, ***P*< 0.01, ****P*< 0.001 and *****P*< 0.0001 versus non-treated cells.

In contrast, the maximum RTX release from NP-APTES-RTX at 0.01 mg Fe/mL obtained in vitro was about 4.5 μM, which decreased cell viability to the same extent as 1 μM of soluble RTX. However, the cellular uptake of NP-APTES-RTX and NP-APTES-PTX after 24 h was only 38 ± 2 pg Fe/cell and 25 ± 3 pg Fe/cell, respectively, meaning that the maximum intracellular level of free RTX or PTX could achieve 2 x 10^{-8} or 7 x 10^{-10} μmol/cell, respectively, if all bound drug would have been released (Fig. 9). These data suggest that the delivery of RTX through NP-APTES-RTX nanoparticles reaches the maximum cytotoxic effect observed with soluble RTX at a lower concentration in A549 cells. These findings support the idea that the lysosomes have the ability to cleave RTX from the nanoparticles, allowing the free RTX to exert its antitumoral effect.

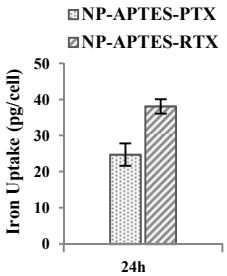

Fig. 9. Cellular uptake of NP-APTES-RTX and NP-APTES-PTX in A549 cells after 24 h of incubation.

The antitumoral effect of the antifolates RTX, PTX or MTX transported into tumor cells through squaramide-functionalized nanoparticles was also studied. Initially, several concentrations

of each squaramide-functionalized nanoparticles (between 0.001 and 0.01 mg Fe/mL) were assayed in A549 cells. As shown in Fig. 10, none of the antifolate-functionalized nanoparticles altered cell viability after 96 h of treatment. Because of the low efficacy we next examined the in vitro cytotoxicity of loaded RTX, PTX or MTX nanoparticles at higher concentrations (between 0.1-1 mg Fe/mL). However, only the highest concentration of loaded RTX nanoparticles (1 mg Fe/mL) exhibited a slight inhibitory effect on cell viability after 96 h of treatment. More concretely, at 1 mg Fe/mL NP-SQ1/RTX reduced cell viability by 20 ± 3%, while NP-SQ2/RTX induced a decrease of 44 ± 3%. The low cytotoxic effect exhibited by these loaded nanoparticles did not seem to be caused by a lower release of bound drug, because at the highest concentration studied (1 mg Fe/mL), the maximum drug release was in the range of 170-190 μM at acidic pH (Table 1). This suggests that the cellular uptake of NP-SQ1/RTX or NP-SQ2/RTX is lower than that of the covalently bound nanoparticles.

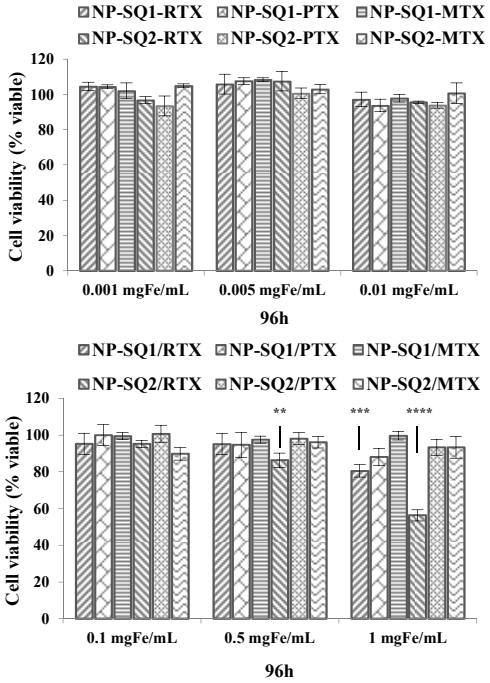

Fig. 10. Determination of cell viability in A549 cells after treatment with NP-SQ1 and NP-SQ2 with RTX, PTX and MTX at different concentrations. The NP concentrations are expressed as mg Fe/mL. Each column represents the mean ± SE of three independent experiments performed in triplicate normalized to non-treated cells (taken as 100%). $^{**}P< 0.01$, $^{***}P< 0.001$ and $^{****}P< 0.0001$ versus non-treated cells.

Previous studies[19] of the interaction between the folic receptor (FR) and FA have demonstrated that the folate pteroate moiety is positioned inside the receptor, whereas its glutamate moiety is solvent-exposed and sticks out of the pocket entrance of the FR. This arrangement allows to those folic acid conjugates through the glutamate residue to interact with FR without adversely affecting this binding.

The covalent binding of the antifolates to the iron oxide nanoparticles described in this work preserved the pteroate residue free to interact with FR. However, in the non-covalent interactions established between the squaramide derivatives and the antifolates, the position of the pteroate moiety is not fixed (Scheme 1). This particular moiety could be placed to the solution, interacting with the squaramides only through electrostatic interactions, or oriented into the squaramide chains. This last disposal disables the interaction with FR preventing the cellular uptake of RTX, PTX or MTX transported by NP-SQ1 or NP-SQ2.

Finally, we suggest that the slight inhibitory effect on cell viability after 96 h of treatment observed for NP-SQ1/RTX and NP-SQ2/RTX at the highest concentration was due to the partial release of RTX in the medium at pH 7.4 and its entrance as soluble drug. Even though we observed this release in the same extent for PTX and MTX, the higher cytotoxic effect of RTX causes the mentioned inhibition.

Importantly, nor unloaded NP-SQ1 and NP-SQ2 nanoparticles neither the nanoparticles functionalized only with DMSA (NP-DMSA), used as negative control, affected cell viability even at the highest iron concentration (1 mg Fe/mL) (Fig. 11), proving that the before mentioned low antitumoral effect was actually induced by the antifolate compounds and not the nanoparticles itselves.

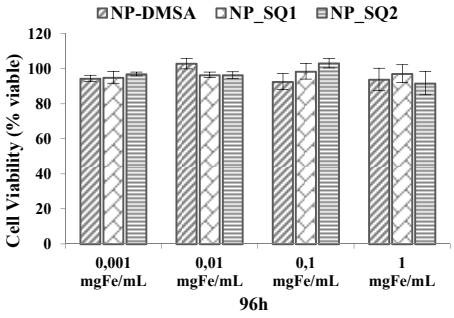

Fig. 11. Determination of cytotoxicity in A549 cells of unloaded NP-DMSA, NP-SQ1 and NP-SQ2 at 96 h.

Experimental

Synthetic procedures

Synthesis of Fe_3O_4 nanoparticles. 0.71g of Fe(acac)3 (2 mmol), 3 mL of oleylamine (6 mmol), 2 mL of oleic acid (6 mmol) and 2.58 g of 1,2-hexadecanediol (10 mmol) were mixed into 20 mL of dibenzylether. The solution was firstly heated at 200 ºC for 1 h and then at 300 ºC for 2 h with vigorous magnetic stirring and reflux under Ar atmosphere. Afterwards, the solution was cooled to room temperature and the nanoparticles were precipitated by adding 25 mL of ethanol to the mixture. The precipitate was collected by centrifugation at 8000 rpm, washed with ethanol (3 x 15 mL) and dispersed in hexane containing 75 mM oleic acid and 75 mM oleylamine.

Synthesis of NP-APTES. 0.5 mL of APTES was added to a colloidal suspension of 25 mg of Fe_3O_4 nanoparticles in 50 mL of toluene anhydride. The mixture was sonicated for 4 h at 60ºC. Finally, the coated Fe_3O_4 nanoparticles were magnetically separated and washed with ethanol (3 x 15 mL) and deionized H_2O (3 x 15 mL).

Synthesis of NP-APTES-RTX or NP-APTES-RTX. 5 mg of RTX or PTX (0.01 mmol) was dissolved in 1 mL of DMSO. The solution was mixed with 2 mL of an aqueous solution of 15.5 mg of 1,3-dicyclohexylcarbodiimide (DCC) (0.075 mmol) and 1.7 mg of N-hydroxysuccinimide (NHS) (0.015 mmol). 10 mg of NP-APTES dissolved in 5 mL of H_2O were added into the above mentioned solution. The pH was adjusted to 8-9 with 1 M NaOH. The final suspension was stirred at 37ºC for 24 h. Finally, the nanoparticles

were isolated with a magnet and washed several times with deionized H_2O.

Synthesis of NP-SQ1 or NP-SQ2. 10 mg of Fe_3O_4 nanoparticles were dispersed in 1 mL of toluene. 40 mg of meso 2,3-dimercaptosuccinic acid (DMSA) (0.22 mmol) and 73.3 mg of SQ1 or 104.6 mg of SQ2 (0.22 mmol) were dissolved in 0.2 mL of DMSO. Both solutions were mixed and sonicated for 5 min before the final solution was stirred for 12h. The nanoparticles were washed with EtOH (3 x 5 mL), MeOH (2 x 5 mL) and acetone (1 x 5 mL) and finally dispersed in 1.2 mL of 0.1% wt NH_4OH.

Synthesis of NP-DMSA. 10 mg of Fe_3O_4 nanoparticles were dispersed in 1 mL of toluene. 40 mg of meso 2,3-dimercaptosuccinic acid (DMSA) was dissolved in 0.2 mL of DMSO. Both solutions were mixed and sonicated for 5 min and then stirred for 12h. The nanoparticles were washed with EtOH (3 x 5 mL), MeOH (2 x 5 mL) and acetone (1 x 5 mL) and finally dispersed in 0.7 mL of 0.1% wt NH_4OH.

Determination of Antifolate retention and release from NP

Analysis of RTX and PTX release from NP-APTES-RTX and NP-APTES-PTX. 0.5 mg of NP-APTES-RTX or NP-APTES-PTX were dispersed in 5 mL of PBS (phosphate buffered saline) buffer (pH=7.4). The pH of the solution was adjusted at 4.0, 5.6 or 7.4 with 1 M HCl. 1 mg of bovine pancreas protease was added into each suspension. The mixture was incubated at 37^{o}C for 24, 48, 72 or 96 h respectively. The nanoparticles were isolated with a magnet and aliquots of 0.5 mL were analyzed by HPLC to determine the release of RTX and PTX from the functionalized nanoparticles. (HPLC conditions: C18 column, Isocratic mode PBS/CH_3CN (80:20), 0.8 mL/min, 30 µL of sample inyected, λRTX: 264 nm, λPTX: 250 nm).

Analysis of RTX, PTX and MTX retained by NP-SQ1 and NP-SQ2. 0.2 mg of NP-SQ1 or NP-SQ2 were dispersed in 0.5 mL of RTX solution (1 x 10-4 M in PBS buffer, pH=7.4) and stirred for 15, 30, 45 or 60 min. The nanoparticles were then isolated with a magnet and washed once with PBS buffer. The resulting solution was filtered and analyzed by HPLC to determine the remaining concentration of RTX. The same procedure was used to determine the retention of PTX and MTX. (HPLC conditions: C18 column, Isocratic mode PBS/CH_3CN (80:20), 0.6 mL/min, 10 µL of sample injected, λRTX: 264 nm, λPTX: 250 nm; λMTX: 303 nm).

Analysis of RTX, PTX and MTX released from NP-SQ1 and NP-SQ2. To perform this analysis, the loaded NP-SQ1 or NP-SQ2 were dispersed in 1 mL of PBS buffer (pH=7.4) and incubated at 37 oC for 24, 48, 72 or 96 h respectively under continuous stirring. The same experiment was performed adjusting the pH at 4.0. The nanoparticles were then isolated with a magnet and washed once with PBS. The resulting solution was filtered and analyzed by HPLC to determine the concentration of RTX, PTX or MTX, (HPLC conditions: C18 column, Isocratic mode PBS/CH_3CN (80:20), 0.6 mL/min, 10 µL of sample injected, λRTX: 264 nm, λPTX: 250 nm, λMTX: 303 nm).

Cell Culture

Cell culture and treatments. A549 human lung adenocarcinoma cells were obtained from the American Type Culture Collection (Manassas, VA). The cells were grown in RPMI 1640 medium supplemented with 2 mM L-glutamine (Sigma-Aldrich, Madrid, Spain), 10% (v/v) fetal bovine serum, 100 units/mL penicillin and 100 µg/mL streptomycin. Tissue culture medium and supplements were purchased from LabClinics S.A. (Barcelona, Spain). When the cells reached 60-70% confluence, vehicle, Raltitrexed (RTX), Pemetrexed (PTX), NP-APTES, NP-APTES-RTX, NP-APTES-PTX, NP-SQ1, NP-SQ1-RTX, NP-SQ1-PTX, NP-SQ1-MTX, NP-SQ2, NP-SQ2-RTX, NP-SQ2-PTX or NP-SQ2-MTX were added to the medium for 24 - 96 h. Stock solutions of RTX and PTX were prepared at 1 mM in phosphate-buffered saline (PBS). Stock solutions of all nanoparticles were prepared at 1 mgFe/mL in phosphate-buffered saline (PBS).

Intracellular Uptake of NP-APTES-RTX and NP-APTES-PTX. A549 cells were plated in 12-well plates at a density of 75 x 10^3 per well in 1.5 mL of growth medium without folic acid (Invitrogen, S.S., Barcelona, Spain) and grown for 24 h. To quantify the cellular uptake, cells were exposed to NP-APTES-RTX and NP-APTES-PTX (0.01 mg Fe/mL) for 24 h. After treatment, cells were washed twice with 1 mL of Versene solution and three times with 1 mL of PBS. The cells were detached with 0.25% trypsin-EDTA, centrifuged and resuspended in 1 mL of PBS supplemented with 10% FBS. 10 µL of the cell suspension was used to count cell number of cell in a Neubauer chamber. The remaining suspension was treated with 100 µL of concentrated HCl and incubated for 1 h at 70^{o}C. Finally, the intracellular iron concentration was determined by inductively coupled plasma atomic emission (ICP-AES) spectroscopy.

Cell culture and Survival/Viability. A549 cells were plated in 96-well plates at a density of 4.5 x 10^3 per well in 200 µL of growth medium without folic acid (Invitrogen, S.S., Barcelona, Spain) and grown for 24 h. To test the efficacy of compounds on cell growth, cells were exposed to RTX (25-1000 nM), PTX (10-1000 nM), NP-APTES-RTX and NP-APTES-PTX (0.001-0.01 mg Fe/mL), NP-SQ1, NP-SQ1-RTX, NP-SQ1-PTX, NP-SQ1-MTX, NP-SQ2, NP-SQ2-RTX, NP-SQ2-PTX and NP-SQ2-MTX (0.001-1 mg Fe/mL) for 24, 48, 72 or 96 h. After treatment, the viability of the cells was measured using the methylthiazoletetrazolium (MTT) method, as previously described by Mosmann.[17] Absorbance was measured at 590/650 nm on an ELISA plate reader (AsysHitech GmbH, Austria). The mean percentage of cell survival relative to that of vehicle-treated cells was calculated from data of three individual experiments performed by triplicate. The results are expressed as the mean ± S.E.M. One-way analysis of variance (ANOVA) followed by Newman-Keuls multiple comparison test was used for statistical evaluations. Differences were considered statistically significant at $P< 0.05$.

Conclusions

In summary four different iron oxide nanoparticles were synthesized and characterized for the delivery of antifolates into cancer cells. These drugs were bound to the nanoparticles by covalent bonding and non-covalent interactions. The cytotoxic assays with A549 cells showed that only one covalent antifolate-functionalized nanoparticle strongly inhibited the viability of these cancer cells.

Acknowledgements

This work was supported by Ministerio de Economía y Competitividad ref. CTQ 2011-27152, Asociación Española contra el Cáncer (Junta de Baleares), Fondos FEDER grant and Conselleria d´ Educació, Cultura i Universitats, Govern de les Illes Balears. Grant FPI09-45692991-H has been selected under an operational program co-financed by the European Social Fund.

Notes and references

[a] Department of Chemistry, University of the Balearic Islands, Cra. de Valldemossa Km. 7.5, 07122 Palma de Mallorca, Balearic Islands, Spain. Fax: 34 971 173 426; Tel: 34 971 172 690; E-mail: jeroni.morey@uib.es

[b] Department of Biology, University of the Balearic Islands, Cra. de Valldemossa Km. 7.5, 07122 Palma de Mallorca, Balearic Islands, Spain.

1 (*a*) J. R. McCarthy and R. Weissleder, *Adv. Drug Deliver. Rev.,* 2008, **60**, 1241; (*b*) C. Sun, J. S. H. Lee and M. Zhang, *Adv. Drug Deliver. Rev.,* 2008, **60**, 1252; (*c*) O. Veiseh, J. W. Gunn and M. Zhang, *Adv. Drug Deliver. Rev.,* 2010, **62**, 284.

2 (*a*) M. Mahmoudi, H. Hofmann, B. Rothen-Rutishauser and A. Petri-Fink, *Chem. Rev.* 2012, **112**; (*b*) V. R. Devadasu, V. Bhardwaj and M. N. V. R. Kumar, *Chem. Rev*., 2013, **113**, 1686.

3 (*a*) F. Sonvico, S. Mornet, S. Vasseur, C. Dubernet, D. Jaillard, J. Degrouard, J. Hoebeke, E. Duguet, P. Colombo and P. Couvreur, *Bioconjug. Chem.,* 2005, **16**, 1181; (*b*) B. Stella, V. Marsaud, S. Arpicco, G. Geraud, L. Cattel, P. Couvreur and J.-M. Renoir, *J. Drug Target.,* 2007, **15**, 146; (*c*) Y. Wang, Y. Wang, J. Xiang and K. Yao, *Biomacromolecules,* 2010, **11**, 3531; (*d*) S. P. Chakraborty, S. K. Mahapatra, S. K. Sahu, P. Pramanik and S. Roy, *Asian Pac. J. Trop. Biomed.,* 2011, **1**, 29; (*e*) G. Zuber, L. Zammut-Italiano, E. Dauty and J.-P. Behr, *Angew. Chem. Int. Ed.,* 2003, **42**, 2666.

4 (*a*) X. Pan and R. Lee, *Expert Opin. Drug Deliv.,* 2004, **1**, 7; (*b*) F. Sirotnak and B. Tolner, *Annu. Rev. Nutr.,* 1999, **19**, 91; (*c*) A. Gabizon, A. Horowitz, D. Goren, D. Tzemach, F. Mandelbaum-Shavit, M. Qazen and S. Zalipsky, *Bioconjug. Chem.,* 1999, **10**, 289; (*d*) S. D. Weitman, R. H. Lark, L. R. Coney, D. W. Fort, V. Frasca and V. R. Zurawski, *Cancer Res.,* 1992, **52**, 3396.

5 (*a*) R. Lee and P. Low, *J.Bio.Chem*., 1994, **269**, 3198; (*b*) C. J. Mathias, S. Wang, R. J. Lee, D. J. Waters, P. S. Low and M. A. Green, *J. Nucl. Med.,* 1996, **37**, 1003.

6 (*a*) N. Kohler, C. Sun, J. Wang and M. Zhang, *Langmuir,* 2005, **21**, 8858; (*b*) K. Wosikowski, E. Biedermann, B. Rattel, N. Breiter, P. Jank, R. Löser, G. Jansen and G. Peters, *Clin.CancerRes.,* 2003, **9**, 1917; (*c*) Y. Zhang, T. Jin and R.-X. Zhuo, *Colloids Surf. B: Biointerf.,* 2005, **44**, 104; (*d*) N. Kohler, C. Sun, A. Fichtenholtz, J. Gunn, C. Fang and M. Zhang, *Small,* 2006, **2**, 785; (*e*) Y.-H. Chen, C.-Y. Tsai, P.-Y. Huang, M.-Y. Chang, P.-C. Cheng, C.-H. Chou, D.-H. Chen, C.-R. Wang, A.-L. Shiau and C.-L. Wu, *Mol. Pharm.,* 2007, **4**, 713; *(f)* R. Dhanikula, A. Argaw, J.-F. Bouchard and P. Hildgen, *Mol. Pharm.,* 2008, **5**, 105; (*g*) X. Yang, Q. Zhang, Y. Wang, H. Chen, H. Zhang, F. Gao and L. Liu, *Colloids Surf. B: Biointerf.,* 2008, **61**, 125; (*h*) M. Davis, Z. Chen and D. Shin, *Nature Rev. Drug Discov.,* 2008, **7**, 771; (*i*) D.-H. Seo, Y.-I. Jeong, D.-G. Kim, M.-J. Jang, M.-K. Jang, J.-W. Nah, *Colloids Surf. B: Biointerf.,* 2009, **69**, 157; *(j)* R. C. Huxford, K. K. E. de, W. S. Boyle, D. Liu and W. Lin, *Chem. Sci.,* 2012, **3**, 198.

7 (*a*) Y.-C. Chen, W.-F. Lee, H.-H. Tsai and W.-Y. Hsieh, *J. Biomed. Mater. Res. Part A,* 2012, **100A**, 1279; (*b*) S. Santra, C. Kaittanis, J. Grimm and J. Perez, *Small,* 2009, **5**, 1862; (*c*) J. Yang, J. Lee, J. Kang, S. J. Oh, H.-J. Ko, J.-H. Son, K. Lee, J.-S. Suh, Y.-M. Huh and S. Haan, *Ad. Mater.,* 2009, **21**, 1

8 (*a*) R. Prohens, G. Martorell, P. Ballester and A. Costa, *Chem. Commun*., 2001, 1456; (*b*) M. N. Piña, M. C. Rotger, A. Costa, P. Ballester and P. M. Deyà, *Tetrahedron Lett*., 2004, **45**, 3749; (*c*) R. I. Storer, C. Aciro and L. H. Jones, *Chem. Soc. Rev.,* 2011, **40**, 2330. (*d*) A. Frontera, J. Morey, A. Oliver, M. N. Piña, D. Quiñonero, A. Costa, P. Ballester, P. M. Deyà and E. V. Anslyn, *J. Org. Chem.,* 2006*,* **71***,* 7185.

9 D. Quiñonero, K. A. López, P. M. Deyà, M. N. Piña and J. Morey, *Eur. J. Org. Chem.,* 2011, 6187.

10 (*a*) S. Sun and H. Zeng, *J. Am. Chem. Soc*., 2002, **124**, 8204; (*b*) S. Sun, H. Zeng, D. B. Robinson, S. Raoux, P. Rice, S. X. Wang and G. Li, *J. Am. Chem. Soc.,* 2004, **126**, 273.

11 M. Ma, Y. Zhang, W. Yu, H.-Y. Shen, H.-Q. Zhang and N. Gu, *Colloids Surf. A: Physicochem. Eng. Asp.,* 2003, **212**, 219.

12 K. A. López, M. N. Piña and J. Morey, *Sens. Actuators B Chem.,* 2013, **181**, 267.

13 K. A. López, M. N. Piña and J. Morey, *Synlett,* 2012, **23**, 2830.

14 (*a*) Z. P. Chen, Y. Zhang, S. Zhang, J. G. Xia, J. W. Liu, K. Xu and N. Gu, *Colloids Surf. A: Physicochem. Eng. Aspects,* 2008, **316**, 210; (*b*) N. Miguel-Sancho, O. Bomatí-Miguel, G. Colom, J.-P. Salvador, M.-P. Marco and J. Santamaría, *Chem. Mater.,* 2011, **23**, 2795; (*c*) A. G. Roca, S. Veintemillas-Verdaguer, M. Port, C. Robic, C. J. Serna and M. P. Morales, *J. Phys. Chem. B,* 2009, **113**, 7033.

15 S. Wang and P. S. Low, *J. Control. Release,* 1998, **53**, 39.

16 J. Arcot, A. Shrestha, *Trends in Food Science and Technology*, 2005, **16**, 253.

17 C. T. Hung, A. D. McLeod, P. K. Gupta, *Drug Dev. Ind. Pharma.,* 1990, **16**, 509.

18 T. Mossmann, *J. Immunol. Methods,* 1983, **65**, 55.

19 C. Chen, J. Ke, X. E. Zhou, W. Yi, J. S. Brunzelle, J. Li, E.-L. Yong, H. E. Xu, K. Melcher, *Nature*, 2013, **500**, 486.

102x36mm (300 x 300 DPI)